International Immunopharmacology 71 (2019) 241–250

Contents lists available at ScienceDirect

International Immunopharmacology

journal homepage: www.elsevier.com/locate/intimp

Dysfunctional microglia:neuron interactions with significant female bias in a developmental gene x environment rodent model of Alzheimer's disease

A.N. vonderEmbse*, Q. Hu, J.C. DeWitt

Department of Pharmacology and Toxicology, Brody School of Medicine at East Carolina University, 600 Moye Blvd., Greenville, NC 27834, USA

ARTICLE INFO

Keywords:
Developmental origin of adult disease
Alzheimer's disease
Microglia
Gene x environment
Neuroimmune

ABSTRACT

Signaling between microglia and neurons is poorly characterized in the pathophysiology of Alzheimer's disease (AD), particularly with regards to gene and environmental (GxE) interactions early in life. This study investigated the maladaptation of microglia:neuron signaling and subsequent susceptibility to neurodegeneration using a developmental origin of adult disease (DOAD) model of AD, characterized previously. Here, we report that postnatal exposure to lead (Pb) in a transgenic (Tg) rodent model of AD resulted in significant female bias consequent to GxE interactions. Atypical, non-neuroprotective microglial phenotypes were observed months after cessation of Pb exposure, as well as evidence for neuronal compensation, that was not observed in WT mice. Specifically, microglia from Pb-exposed Tg (GxE) females exhibited atypical polarization profiles for activation earlier and more severely than males and WT mice, that persisted over time to become contextually maladaptive. By postnatal day (PND) 240, microglia from GxE females also sequestered less neurotoxic iron in the hippocampus. In the same GxE female population, measures of neuronal parameters, such as hippocampal TrkB expression, revealed evidence of disharmonious and compensatory interactions with microglia within the pathological progression. Likewise, GxE interactions resulted in female-biased, late-life changes to key synaptic proteins crucial to synapse dynamics and microglial signaling. These incongruent microglia:neuronal dynamics were observed in GxE males at later ages compared to females, and not observed in either gene- or environment-only populations. Altogether, our results support a gene x environment model of female-biased microglial susceptibility to later-life development of AD, and highlight markers for maladaptive microglia:neuron signaling and compensation.

1. Introduction

The etiology of neurodegenerative diseases, like Alzheimer's disease (AD), may stem from atypical brain development, in a variation on the developmental origin of adult disease (DOAD) hypothesis [1]. Women are disproportionally affected by AD [2], and progress faster to disease and decline at a higher rate than men [3,4]. Subsets of other sex-biased CNS diseases, such as autism spectrum disorders and schizophrenia, have been traced back to aberrations at distinct stages of sexually dimorphic brain development and sex-specific gene expression therein [5]. Moreover, studies of early-life immune activation demonstrate persistent effects of atypical brain development on later-life cognitive endpoints and sex biases [6,7]. As the resident innate immune cells of the central nervous system (CNS), microglia have been implicated in several nervous system disorders, but the correlation between early postnatal microglial dysfunction and the exacerbation of later-life, sex-biased neurodegeneration is not well understood.

In the etiopathology of complex diseases that involve potential lifelong immune dysfunction, temporal waves of compensation are likely to play a more significant role than have previously been reported in the literature. The transition from adaptive to maladaptive responses characteristic of a lifelong etiology is of particular importance for studies involving microglia, which are critical to development, neuronal homeostasis, and neurogenesis. We have previously reported that postnatal exposure to a model neurotoxicant, lead acetate (Pb), not only preferentially increased disease susceptibility in females, but also correlated with decreased microglial activation [8]. This suggests a gene x environment-mediated vulnerability related to microglial neglect or dysfunction may be consequent to interference with the closure of a critical window of development for integrated microglia and neuronal maturation, persisting into adulthood. Furthermore, as this relatively acute, low dose exposure was severe enough to exacerbate AD pathologies and alter microglia months after exposure cessation, the exposure paradigm is more analogous to the formation of unfavorable

* Corresponding author at: Department of Molecular Biosciences, University of California at Davis, One Shields Ave, Davis, CA, USA.
E-mail addresses: anvonderembse@ucdavis.edu (A.N. vonderEmbse), huq@ecu.edu (Q. Hu), dewittj@ecu.edu (J.C. DeWitt).

https://doi.org/10.1016/j.intimp.2019.03.039
Received 5 October 2018; Received in revised form 9 March 2019; Accepted 20 March 2019
Available online 27 March 2019
1567-5769/ © 2019 Elsevier B.V. All rights reserved.

developmental conditions promoting adaptation for survival, warranting further exploration into temporal changes in microglia-neuron interactions.

The postnatal exposure window utilized in this study corresponds to a critical window of development for neuronal and microglial maturation, as well as maturation of synaptic receptors in the hippocampus critical to long term potentiation (LTP), synaptic plasticity, and adult neurogenesis [9,10]. Perturbation of this dual learning and maturation period via low level toxicant exposure may critically and persistently alter the neuroimmune parenchyma; beyond interfering with closure of this critical window of development, the resulting phenotype could manifest as abnormal neuronal wiring patterns, atypical epigenetic regulation, and/or re-patterned functional phenotypes.

In the current study, we investigated patterns of timing and fluctuation for hallmarks of microglial function and synapse dishomeostasis, considered to be one of the earliest molecular pathologies in AD [11,12]. To assess beneficial vs detrimental adaptation, the severity and timing of neurosupportive microglial endpoints were analyzed, as well as correlative neuronal markers at various time points. This study tested the hypothesis that the combination of both genetic proclivity and postnatal toxicant exposure, as a DOAD model of gene x environment interactions, would alter the severity or onset of AD-related synaptic aberrations consequent to dysfunctional microglia with a significant female bias. The purpose of the current study was to delineate markers of dysfunction in microglia:neuron crosstalk originating during atypical development, and integrating the timeline of maladaptation to known pathological markers in a genetic model of AD. By utilizing this model of postnatal gene x environment interactions, we propose a novel analysis of early, sexually dimorphic microglial dysfunction in AD and interrelated functional endpoints with synaptic aberrations.

2. Materials and methods

2.1. Animal handling

All experimental animal handling and dosing was carried out in accordance with procedures approved by the East Carolina University Institutional Animal Care and Use Committee (IACUC). Pregnant wildtype (SFN) and transgenic dams (3xTgAD; B6; 129-*Psen1*^{tm1Mpm}Tg (APPSwe,tauP301L)1Lfa/Mmjax) were obtained from the seed colony in the ECU Department of Comparative Medicine and kept on a 12:12 hour light/dark cycle, with access to food and water ad libitum. Litters were culled to eight after birth (postnatal day, PND 1), weaned at PND 21, and separated by sex into cages of no more than four animals/cage.

2.2. Dosing and tissue preparation

Dosing solutions of lead acetate (100 ppm) dissolved in sterile water were prepared weekly. From PND 5–10 neonates were dosed with lead acetate or vehicle once per day using a modified gavage technique [13]. One mouse per sex, litter, and treatment group was randomly selected and euthanized at PND 120, 180, or 240. As per ethical use protocol, animals were euthanized with isoflurane followed by decapitation, and the brain was carefully removed and hippocampi dissected in ice cold phosphate buffered saline (PBS). For histochemical analysis the left hippocampi was fixed for 24 h in 10% neutral buffered formalin followed by 70% ethyl alcohol before paraffin fixation. For flow cytometric analysis, the remaining left hemisphere sans hippocampus was placed in FACS buffer (3% fetal calf serum (FCS), 0.1% sodium azide, and 10 mM ethylenediaminetetraacetic acid (EDTA) in PBS) for subsequent homogenization. The right hemisphere and cerebellum were minced and slowly frozen in cryopreserve (0.32 M sucrose, 10% dimethyl sulfoxide (DMSO), PBS) for later Western blot analysis.

2.3. Flow cytometry

Papain (~200 U/mL) was activated 30 min prior to use at 37 °C with activation buffer (1.1 mM EDTA, 0.067 mM β-mercaptoethanol, 5.5 mM L-cysteine). The left hemisphere sans hippocampus was gently minced and enzymatically digested with activated papain (20 U/mL) for 20 min at 37 °C. Enzyme halt buffer (20% FBS, PBS) was added, and the homogenate was filtered through a 70 μm nylon mesh filter before centrifugation at 1000*g* for 5 min. Myelin removal was accomplished via resuspension in 30% isotonic Percoll (GE Healthcare, Uppsala, Sweden) and centrifugation at 500*g* for 20 min. Brain homogenates sans myelin were then resuspended in RBC Lysis Bufer (eBioscience, San Diego, CA, USA) for 10 min and passed through a 40 μm nylon mesh filter. Briefly, cells were washed with FACS buffer (3% FCS, 0.1% sodium azide, 120 mM EDTA) twice with a series of resuspensions and centrifugations at 1000*g* for 5 min. Following analysis for yield and viability, samples were aliquoted to 1×10^5 cells/tube in incubation buffer (10% FBS, PBS) for 30 min on ice. The following primary antibodies (1:100) were added for 30 min at 4 °C, protected from light: CD86-PE and CD209-APC (Abcam). Following incubation, cells were washed with PBS and centrifuged at 350*g* for 5 min, resuspended in PBS, and read using a BD Accuri C6 flow cytometer (BD Biosciences, Franklin Lakes, NJ, USA). A total of 10,000 events were recorded per sample. Doublet exclusion and live/dead gating was performed, and quadrant crosshairs were determined via fluorescence minus one (FMO) positive controls. The data are represented as the fold change of the % CD86- or CD209-positive cells.

2.4. Immunohistochemistry

Formalin-fixed, paraffin-embedded (FFPE) hippocampi were sliced on a rotary microtome at 16 μm and mounted on Superfrost Plus slides (Azer Scientific, Germany). Briefly, slides were dewaxed in Histo-Clear II (Electron Microscopy Sciences, Halfield, PA), followed by washes in 100% and 95% ethyl alcohol and PBS. Antigen unmasking was accomplished using a heat-mediated citrate buffer, followed by incubation in 0.3% hydrogen peroxide for 30 min. All subsequent staining was performed using Sequenza-Coverplate racks (Thermo Scientific, Waldorf, Germany). Sections were permeabilized with PBS with Tween 20 (TPBS) and blocked with diluted normal serum (ABC Vectastain; Vector Laboratories, Burlingame, CA, USA). Slides were then incubated with anti-ferritin primary antibody (1:1000; Abcam, Cambridge, MA, USA), for 60 min at room temperature or overnight at 4 °C. Sections were visualized using ABC Vectastain and diaminobenzidine (DAB) kits (Vector Laboratories) and counterstained with Harris' Alum Hematoxylin. After sequential washing in ethyl alcohol and Histo-Clear, slides were coverslipped with Permount (Fisher Scientific, Fair Lawn, NJ, USA) and cured overnight prior to visualization.

Slides were visualized using a Leica DM1000 light microscope at 20× magnification with a SPOT™ Idea camera attachment and Advanced Imaging software. Two regions of interest (ROI) per animal were chosen at random along the dentate gyrus, with the viewing frame containing as much tissue as possible. Immunopositive ferritin reactivity was determined via FIJI [14] analysis over a predetermined background threshold and color deconvolution. The % area ferritin positive/ROI was determined and averaged per animal, and results are represented as the mean ± SEM.

2.5. Immunofluorescence

Slide dewaxing, rehydration, and antigen retrieval was performed in a similar manner to immunohistochemistry. Following insertion into the Sequenza racks and two-5 min washes with TPBS, slides were incubated with blocking buffer (10% donkey serum, 0.1% Triton X-100, PBS) for 60 min at room temperature. Overnight incubation at 4 °C was carried out with the primary antibody cocktail, diluted in blocking

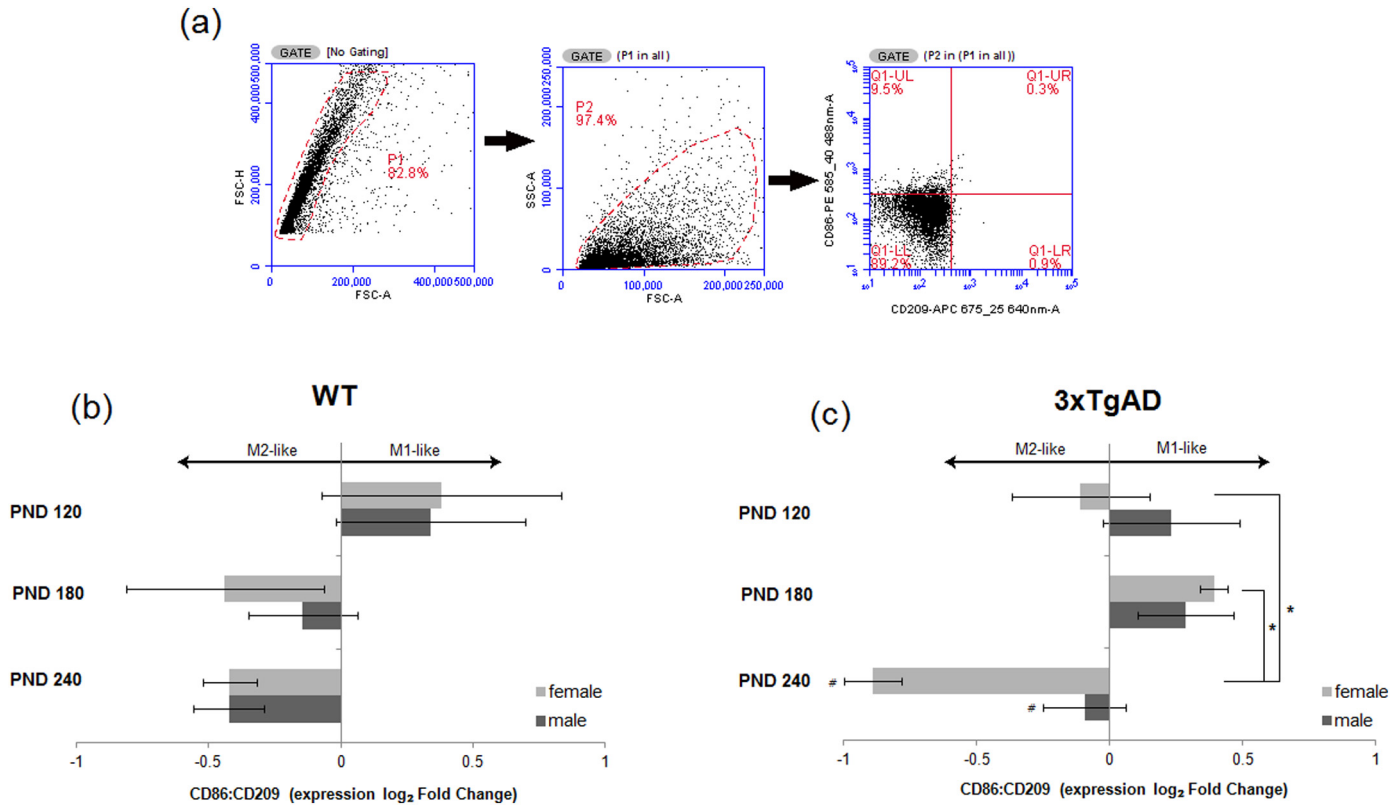

Fig. 1. Developmental Pb exposure persistently altered microglial polarization profiles, varying with sex and mouse strain. (a) Representative gating schematic and flow cytometry output plots. (b,c) Quantification of CD86:CD209 expression ratio as mean ± SEM log-transformed fold changes over to age-, sex-, and strain-matched controls. n = 3–9 mice/sex/age/treatment/strain. $p < 0.05$ was considered statistically significant. * = significant among ages. # = significant between sex. PND: postnatal day, WT: wildtype, FSC: forward scatter, SSC: side scatter.

buffer: tyrosine kinase B (TrkB) (4 µg/mL, rabbit anti-mouse IgG; Abcam) and ionized calcium binding adaptor molecule 1 (Iba1) (1:200, goat anti-mouse pAb; Abcam). Sections were washed twice with TPBS, and the secondary antibody cocktail, diluted in TPBS, was applied for 60 min protected from light: AlexaFluor555-conjugated donkey anti-rabbit (1:500, Abcam) and FITC-conjugated donkey anti-goat (1:500, Abcam). Nuclei were stained with 4′,6-diamidino-2-phenylindole (DAPI, 1.5 µM; Life Technologies, Eugene, OR, USA) and, after two washes with PBS, treated with TrueBlack Lipofuscin Autofluorescence Quencher (Biotium, Fremont, CA, USA) for 30 s. Briefly, slides were washed and coverslipped with ProLong Gold antifade reagent (Life Technologies), left to cure for 24 h, and stored upright protected from light.

Hippocampal sections were visualized with a Zeiss LSM 700 laser scanning confocal microscope with the EC Plan-Neofluar 10x/0.30 M27 objective. The dentate gyrus (DG) and CA3 region were identified based on standardized hippocampal landmarks, and two counting frames per region (150 µm × 97 µm) were used as the ROI. Co-localization of TrkB with Iba1 was excluded from analysis, and fluorescence intensity was considered positive over a predetermined threshold above background fluorescence. Data are represented as mean relative fluorescence intensity ± SEM.

2.6. Western blot

2.6.1. Synaptosome preparation

Crude synaptosomal fractions (P-2) were prepared from minced, cryopreserved right hemispheres and cerebellums. Frozen tissue was quickly thawed in a warm water bath and centrifuged at 1000g for 5 min at 4 °C. The supernatant was discarded and the pellet was re-suspended in homogenization buffer, consisting of protease inhibitor cocktail (Halt™ Single-Use, Thermo Scientific, Rockford, IL, USA), three parts PBS, and one part 4× Gradient Buffer (1.28 M sucrose, 4 mM EDTA, 20 mM Tris, pH 7.4). Briefly, tissue was homogenized in a chilled 15 mL Tenbroeck glass homogenizer and centrifuged at 1000g for 10 min. The supernatant was then collected and further centrifuged at 10,000g for 20 min, and the remaining pellet was considered the P-2 synaptosome fraction. Aliquots of the P-2 fraction were either immediately analyzed or routinely cryopreserved at −80 °C until further analysis.

2.6.2. Protein concentration and Western blotting analysis

The P-2 fraction was resuspended in PBS and total protein concentration was determined with BCA Protein Assay (Thermo Scientific). Synaptosomes were diluted to 10 µg/mL in NuPAGE LDS reducing agent, LDS sample buffer (Invitrogen, Carlsbad, CA, USA), and denatured on a 70 °C heating block for 10 min. Samples were then electrophoresed on 10% Bis-Tris Mini Gels (Invitrogen) and transferred onto a 0.45 µm nitrocellulose membrane. Following overnight incubation with constant agitation in blocking buffer (Rockland, Gilbertsville, PA, USA), membranes were probed for 1 h with the appropriate primary antibodies (Abcam) in blocking buffer with 0.1% Tween-20: either SNAP25 (0.02 µg/mL, goat pAb) or synaptophysin (1:500, mouse mAb) with beta actin (1:10,000, rabbit pAb). Membranes were washed four times with TPBS for 5 min each and incubated for 1 h with the cognate secondary antibody cocktail (1:25,000; Li-Cor, Lincoln, NE, USA) diluted in blocking buffer and 0.1% Tween-20: either donkey anti-rabbit IRDye 680RD and donkey anti-goat IRDye 800CW, or goat anti-rabbit IRDye 680RD and goat anti-mouse IRDye 800CW. Membranes were washed four times with TPBS and once with PBS for 5 min each, left to dry for at least 24 h, and read on a Li-Cor Odyssey CLx. Densitometric quantification was performed using Li-Cor Image Studio™. Results are

expressed as fold change over sex- and age-matched vehicle-treated controls corrected for equal loading to beta actin.

2.7. Statistics

All statistical analyses were performed using Statistical Analysis System (SAS Institute, Cary, NC, USA). Two-way analysis of variance (ANOVA) for sex and age effects was performed for each strain for microglial polarization, treatment and sex effects for each age and strain for ferritin and TrkB analysis, and treatment and age effects for each sex for synaptic protein expression. Individual pairwise comparisons were made with a *t*-test or a Tukey's studentized range distribution method. All data in bar charts are represented as mean ± SEM. $p < 0.05$ was used to denote statistical significance.

3. Results

3.1. Pb-associated changes in microglial polarization profiles varied depending on sex and genetic proclivity for AD

Microglia were characterized from whole brain homogenates via flow cytometry to evaluate functional alterations in activation profiles using CD86 and CD209 as M1- and M2-associated surface markers, respectively (Fig. 1a). The M1:M2 ratio was used to characterize microglial activation skewed towards a more pro-inflammatory, M1-like or anti-inflammatory, M2-like profile. At PND 120, all male mice postnatally exposed to Pb, regardless of strain, exhibited an M1-skewed microglial phenotype compared to controls, whereas Pb-exposed female mice of the same age exhibited a modest trend towards an M2-like phenotype when given a genetic proclivity for AD (Fig. 1b, c). Pb-exposed WT mice followed the general microglial activation time course typical for pathologic or neurotoxic stimuli from M1 to M2 over time [15,16] with little variation due to sex (Fig. 1b). However, in their Tg counterparts, Pb exposure resulted in a more delayed transition to M2-skewed polarization, with the M1 skew lasting until PND 180 (Fig. 1c). By PND 240, Pb-exposed Tg females exhibited a significantly stronger M2 skew than males (Fig. 1c). Likewise, the microglial activation profile for Pb-exposed Tg female microglia at PND 240 was significantly more polarized towards M2 than younger Tg females.

3.2. Pb exposure persistently altered hippocampal ferritin expression in 3xTgAD mice compared to WT, and varied over time depending on sex

Immunohistochemical analysis of hippocampal ferritin expression revealed a high degree of specificity for localization within the CA3 (Fig. 2a) and hilar regions, overlapping with the mossy fiber pathway. Along with positive cellular immunostaining, ferritin was also observed to aggregate in atypical crystallite fragments (Fig. 2b, c) throughout the hippocampus, indicative of degradation and dysfunctional iron sequestration [17].

Quantification of CA3 ferritin immunolabeling in WT mice showed no significant changes consequent to Pb exposure, and only a modest Pb-associated increase at PND 120 in both sexes (Fig. 2e). Conversely, sex and/or treatment effects were detectable in Tg mice at all ages. Ferritin expression in vehicle-treated Tg mice did not vary by sex at either PND 120 or 180, but at PND 240 was significantly decreased in males compared to females (Fig. 2g).

Pb exposure in Tg mice significantly increased ferritin expression at PND 120, and was higher in males than females (Fig. 2e). The Pb-associated increase persisted to PND 180 in both Tg sexes, but was not seen in WT mice of the same age (Fig. 2f). By PND 240, only Pb-exposed Tg males exhibited increased hippocampal ferritin immunolabeling when compared to females as well as vehicle-treated controls (Fig. 2g).

3.3. TrkB expression in the CA3 hippocampal subregion is reduced over time in a sex-dependent manner

Functional characterization of microglial neurosupportive trophic signaling was identified through immunohistochemical staining for TrkB in the hippocampal CA3 region, quantified as non-microglial TrkB immunolabeling through omission of co-localization with Iba1, a general microglial marker (Fig. 3a, b).

Parallel trends were observed in both WT and Tg males over time for Pb-associated changes in non-microglial TrkB expression. Pb exposure significantly increased TrkB expression in males at PND 120, followed by a decrease by PND 240 that was significant compared to vehicle-treated controls in Tg males (Fig. 3c, d).

In WT females, Pb exposure resulted in decreased TrkB expression at PND 120 compared to vehicle-treated controls that then persisted to PND 240 (Fig. 3c). However, Tg females exposed to Pb exhibited significantly higher TrkB expression at PND 120 that was significantly decreased by PND 240, but not when compared to vehicle-treated controls (Fig. 3d).

3.4. Changes in synaptic protein expression was observed earlier and more extensively in Tg females compared to males following postnatal Pb exposure

Western blotting of Tg whole brain synaptosomal isolates for the presynaptic proteins synaptophysin and SNAP25 revealed significant changes related to developmental Pb exposure at PND 120 and 240 that varied with sex. In Tg females, both synaptic proteins measured were significantly reduced in Pb-exposed females compared to vehicle-treated controls at PND 120 and expression increased over time, with a significant Pb-associated increase in SNAP25 expression by PND 240 (Fig. 4a,c).

Comparatively, Pb-exposed Tg males had significant reductions only in synaptophysin at PND 120 (Fig. 4d), while SNAP25 remained relatively unaffected (Fig. 4b). By PND 240, Pb exposure significantly decreased expression of both synaptic proteins (Fig. 4b, d), in direct opposition to the increase seen in females at this latest time point. Interestingly, at PND 240, blots probed for SNAP25 revealed the presence of potential cleavage products in both male and female mice regardless of treatment (Fig. 4a, b), a trend which was observed in all replicates and deemed unlikely to be caused by technical issues, such as improper handing or degradation.

4. Discussion

In the etiological inquisition of AD, early synaptic dysfunction is still incompletely understood, and even less is known about how early-life exposure to toxicants contributes to or initiates this pathological phenomenon. We've previously reported that postnatal Pb exposure in a 3xTgAD mouse model of AD increased susceptibility to amyloid accumulation in females, correlating with decreased microglial activation months after exposure cessation [8]. It is thought that microglia become activated in the presence of amyloid-β to promote phagocytosis and clearance [18], suggesting that the observed reduced activation and accumulation of amyloid is indicative of dysfunctional microglia and long-term, atypical interactions with neurons. In this study, we investigated the extent and severity of microglial dysfunction and neuronal impact later in life, as well as the persistence of the female sex bias within a similar gene x environmental model for the developmental origins of AD. Our results corroborate the initial hypothesis that perturbations to genes and the developing environment act synergistically to disrupt markers of healthy microglia:neuron interactions later in life, and do so with detectable sex bias.

Importantly, the GxE female-biased interactions between microglia and neurons varied temporally, effectively forming a rough time course of the maladapted interactions between the two cell types, whether due to compensation, metabolic exhaustion, or even aging. Furthermore,

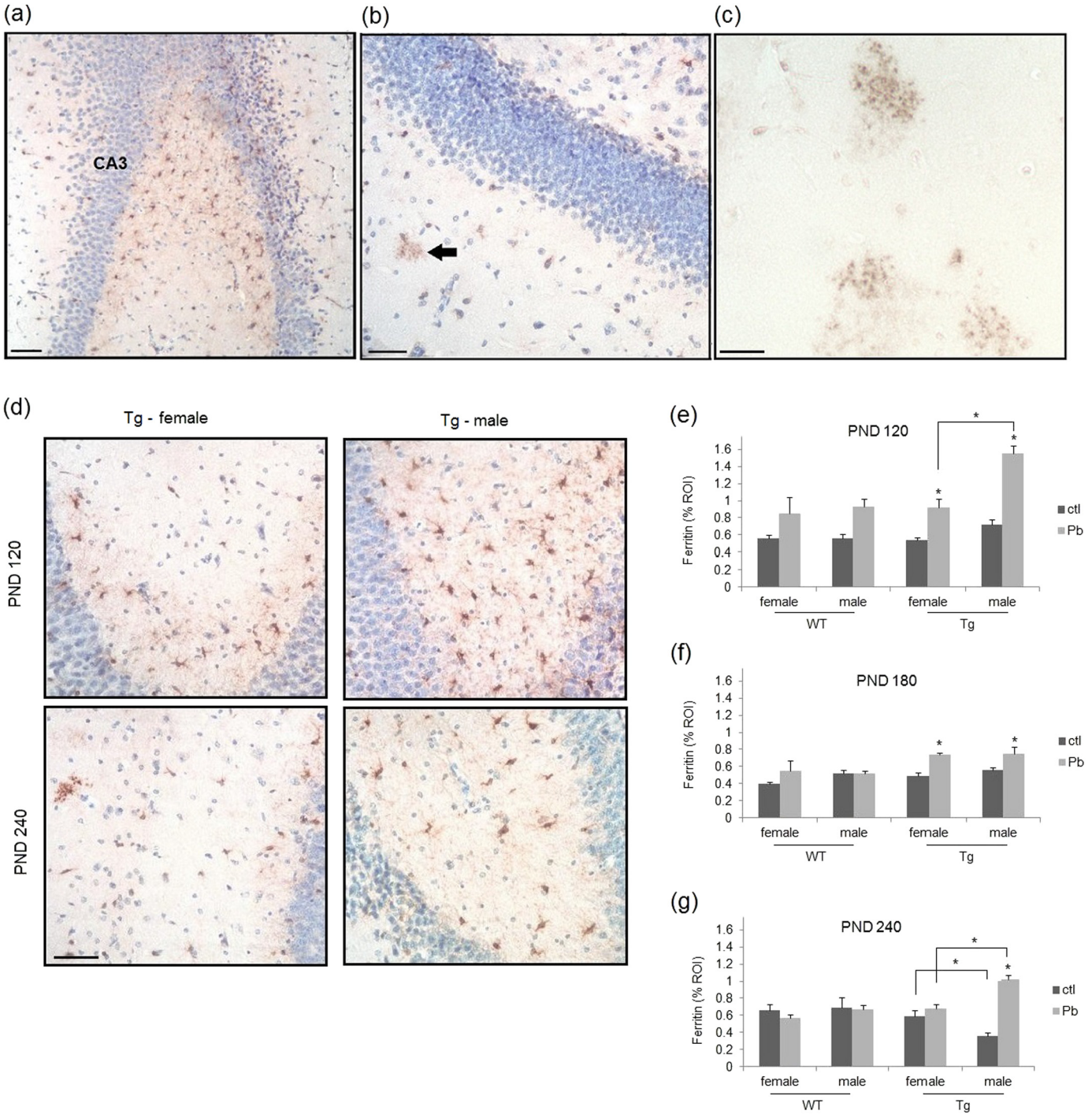

Fig. 2. Hippocampal ferritin expression was persistently altered in Tg mice, more so in males compared to females. Representative images depicting localization of ferritin immunoreactivity in the CA3 hippocampal region (a), and accumulation of fragmented ferritin aggregates (b–c). (d) Representative images of Pb-exposed Tg female and male hippocampal CA3 regions at PND 120 (top row) and PND 240 (bottom row). Ferritin immunoreactivity within the CA3 region of interest (ROI) was quantified at PND 120 (e), PND 180 (f), and PND 240 (g), expressed as mean % ROI ± SEM. n = 3–10 mice/sex/age/treatment/strain (e–g). *$p < 0.05$ was considered statistically significant. Scale bar = 70 μm (a), 44 μm (b), 6 μm (c), and 60 μm (d). PND: postnatal day, ROI: region of interest, WT: wildtype, Tg: 3xTgAD transgenic, ctl: control.

the temporal variability of the data highlights the importance of experimental timing for etiologic evaluation of the neuroimmune system in AD, as well as cautious interpretation of pathophysiological roles, particularly for microglia, at single time points in a long and heterogeneous disease progression. In utilizing three terminal endpoints the present study was able to evaluate not only the temporal changes to GxE-related effects, but also more clearly delineate the genetic "G"-specific effects at an age of early adulthood in WT mice that's relatively independent of the confounding variable of aging.

Another important finding from the present study was the potentiative effect of developmental Pb exposure with the genetic proclivity to AD on the various microglial and neuronal parameters measured, in support of the study's hypothesis. Additionally, GxE interactions produced significant sex differences in microglial phenotypes. Microglia from Pb-exposed Tg mice differed significantly between males and females at PND 180 and 240 in terms of activated

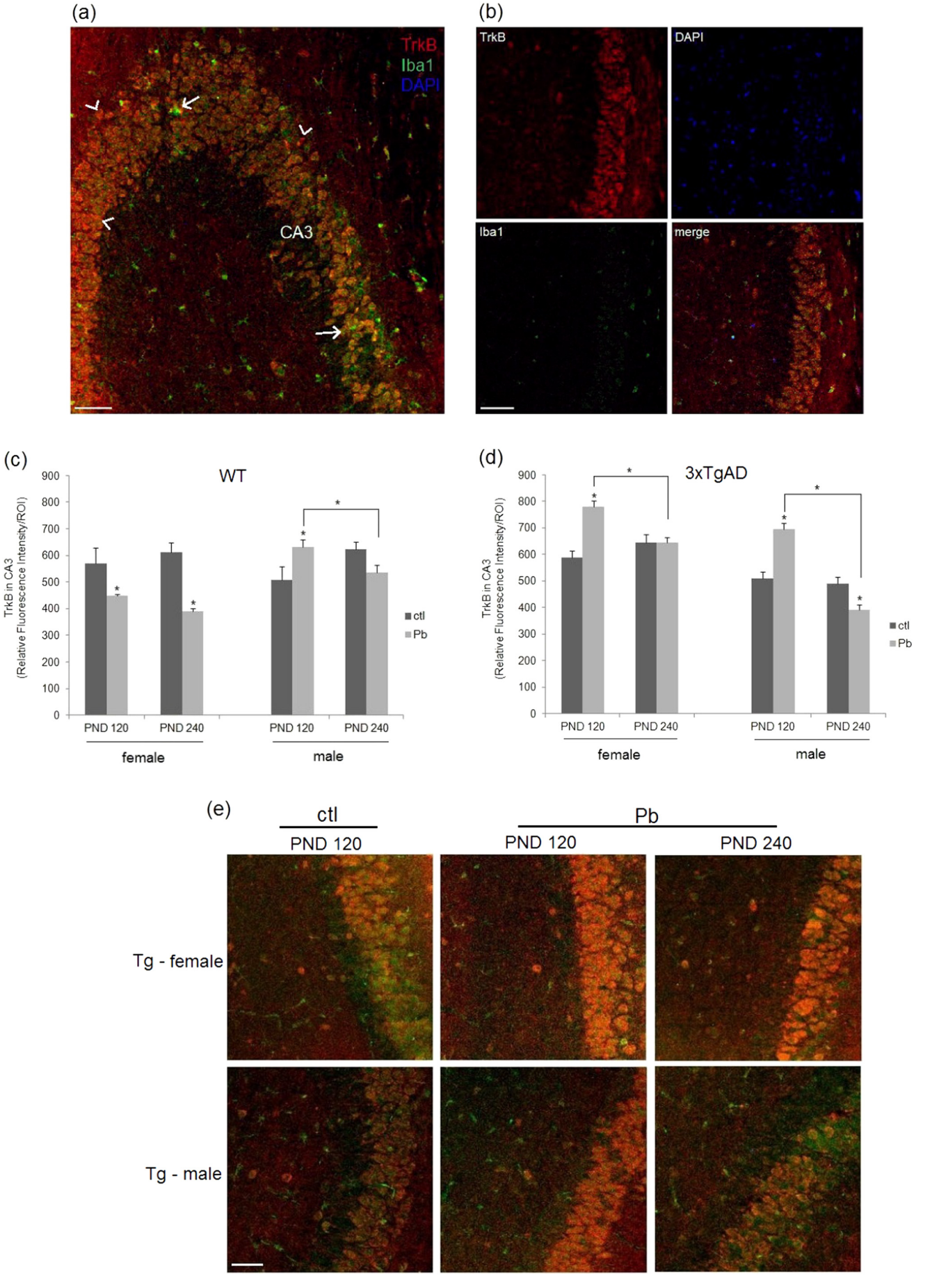

(caption on next page)

Fig. 3. TrkB expression in the CA3 region was increased by Pb exposure compared to controls at PND 120 in all groups except WT females, and decreased at PND 240 in all groups except Tg females. (a) Immunofluorescent staining within the hippocampal CA3 region for positive TrkB immunoreactivity in microglial (arrow) and non-microglial (arrow heads) cells. (b) Representative images of TrkB (red) and the microglial marker Iba1 (green), and DAPI-stained nuclei (blue). TrkB expression was quantified in non-microglial cells as $TrkB^{+}/Iba1^{-}$ at PND 120 and 240 in WT (c) and Tg (d) mice. Representative images of hippocampal TrkB expression in Tg females (e, top row) and Tg males (e, bottom row). Data are represented as mean relative fluorescence intensity per ROI ± SEM. n = 3–5 mice/sex/age/treatment. Scale bar = 73 μm (a), 95 μm (b), and 54 μm (e). *$p < 0.05$ was considered statistically significant. PND: postnatal day, ctl: control, ROI: region of interest. (For interpretation of the references to color in this figure legend, the reader is referred to the web version of this article.)

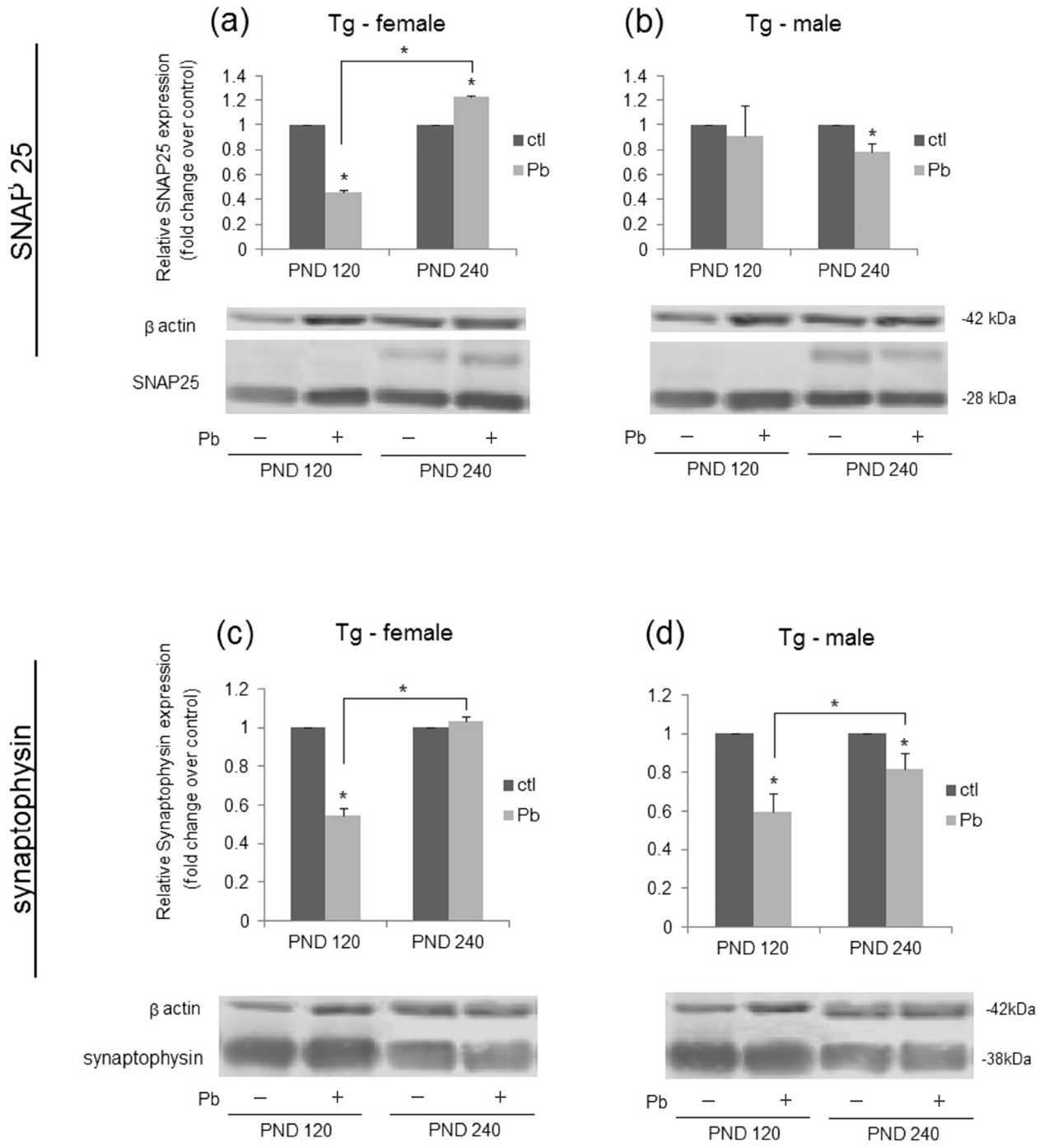

Fig. 4. Synapse-related proteins SNAP25 and synaptophysin were decreased compared to controls at PND 120 in Pb-exposed Tg females and PND 240 in Pb-exposed Tg males. Quantification and representative western blots for synaptosomal SNAP25 (a–b) and synaptophysin (c–d) expression in 3xTgAD females (a,c) and males (b,d). Data are represented as mean fold change over sex- and age-matched controls ± SEM. n = 3 mice/sex/age/treatment. *$p < 0.05$ was considered statistically significant. PND: postnatal day, ctl: control.

polarization ratios (Fig. 1c), and PND 120 and 240 for iron sequestration (Fig. 2e, g). These sex differences were anticipated for microglia function due to the timing of Pb exposure coinciding with a sexually dimorphic critical window of microglial development [7]. Individually, Pb-exposed WT mice representing the environmental 'E' component exhibited no microglial sex differences, whereas control-treated Tg mice representing the 'G' component only had sex differences in both microglial polarization skew and iron sequestration at PND 240, an age of obvious disease pathology in this mouse model (Figs. 1 and 2). This would suggest GxE interactions not only promoted sex differences for two microglial parameters important for neuronal interactions in AD, but also acted synergistically to induce these microglial sex differences earlier, as seen in Pb-exposed Tg mice at PND 120 (Figs. 1c and 2g).

Of particular interest was the strong M2 skew in microglial polarization at PND 240 for Pb-exposed Tg females (Fig. 1c). Following pathologic stimuli, microglia drastically changes functional phenotype to adopt an activated state congruent with the type, strength, and duration of the stimulus [19]. This polarized activation, although not discriminately bifurcated, can be analyzed by the ratio of the two most general forms of macrophage activation, M1:M2, or expression of CD86:CD209, respectively. This relative ratio of polarization is more likely indicative of microglial responsiveness to alterations to the microenvironment than absolute levels of either CD86 or CD209, particularly when considering the heterogeneity of the cell population and specific demands of the CNS [20]. Similarly, numerous studies have identified upregulation of both M1 and M2 associated genes in CNS disease and neurodegeneration [15,21–23], highlighting the complexity of microglial response in AD. The prolonged M2 phenotype has been correlated with both immune "priming" [24] and a type of "innate immune memory" [25] that persists following systemic infection or inflammation and ultimately contributes to chronic neurodegeneration. Chronic, strong M2-polarized microglial activation profiles, seen in Pb-exposed Tg females at PND 240 (Fig. 1c), are particularly detrimental in neurodegenerative diseases for two reasons, the first being a lack of appropriate, strictly regulated M1/M2 activation balance concordant with region-specific signals derived from the immediate microenvironment. The second reason, later-life, strong M2 polarization, would be considered a damaging phenotype in our model due to the resultant decreased pool of ramified microglia. In a recent study, the presence of mature, ramified microglia was shown to be neuroprotective in NMDA-induced hippocampal excitotoxicity, whereas microglial activation coincided with regional neuronal vulnerability; region-specific vulnerability occurred to a greater extent than is accounted for by endogenous glutamate receptor variability [26]. Taken together, GxE interactions promoted female-biased microglial activation profiles associated with atypical and non-neuroprotective functionality that were exacerbated with age.

Microglial iron sequestration, measured as hippocampal region-specific ferritin immunopositive staining, was also exacerbated by GxE interactions with detrimental female bias. At PND 120, hippocampal ferritin expression was significantly elevated in Pb exposed Tg mice, more so in males than females (Fig. 2e). The Pb-associated increase in ferritin persisted to PND 180 (Fig. 2f), but by PND 240 Tg sex differences re-emerged (Fig. 2g). Even though Pb exposure did not alter Tg female ferritin compared to vehicle-treated controls at PND 240 (Fig. 2g), the interpretation is not the same at the similar ferritin levels between ctl- and Pb-treated WT counterparts. This is due to the identification of microglial ferritin expression as a neuroprotective function, specifically in an amyloid-accumulating AD brain. Ferritin is an iron metabolism molecule, comprised of a multi-subunit protein shell with a ferroxidase center [27]. The ferritin in neurons, rich in H-chain subunits, is involved in the detoxification of ferrous ion (Fe^{2+}), whereas ferritin expressed in a subset of martyr microglia, rich in L-chain subunits, possess glutamate residues to facilitate sequestration and long-term storage of excess extracellular iron [28]. Notably, ferritin and amyloid precursor protein (APP) mRNAs are induced by similar translational mechanisms, and both metalloproteins are upregulated as neuroprotective compensation against oxidative stress and acute IL-1 [29]. Ferritin has been shown to promote the rapid transition of microglial activation states from M2 to M1 [30], a trend replicated over time in microglia from Pb-exposed WT mice (Figs. 1b and 2e–g). However, there is less correlation between the two microglial parameters in Tg mice. Although Pb-exposed Tg males gradually lose the correlation over time, Pb-exposed Tg females exhibit far more atypical, inverse correlations between M1 skew and increased ferritin from PND 120 to 180 and a strikingly exaggerated M2 response at PND 240 even with ferritin levels comparable with WT mice (Fig. 2g).

One potential explanation is the pathological accumulation of amyloid that is characteristic in these 3xTgAD mice that would then alter the efficacy of finely balanced intrinsic neuroprotective mechanisms or overload microglia already burdened with early iron sequestration. Increased ferritin expression at PND 240 in Pb-exposed Tg males (Fig. 2g) infers male microglia were still responsive to excess, neurotoxic iron occurring fairly late in this rodent model's disease progression, likely linked to amyloid accumulation. The lack of ferritin expression in Pb-exposed Tg females at PND 240 (Fig. 2g) suggests any amyloid accumulation was not stimulating an efficacious ferritin response in these microglia. This interpretation is corroborated by the presence of crystallite ferritin immunopositive fragments (Fig. 2b, c) that were frequently observed in these mice (Fig. 2d, bottom left panel) (data not shown), indicative of ferritin degradation and release of intracellular neurotoxic iron. Indeed, preferential, microglia-directed damage or even necrosis can occur in ferritin-positive, M1-activated microglia due to the interaction of M1-specific superoxides and release iron via the Fenton reaction [30], incriminating the GxE-associated striking increase in ferritin at PND 120 (Fig. 2e). Additionally, ferritin can become dysfunctional over time, eventually degrading into crystallite hemosiderin and releasing iron into the immediate vicinity [17], even without the prompting from M1-associated superoxides. Although additional analysis is required to determine the extent of hippocampal ferritin degradation associated with GxE interactions, the presence of these fragments may have erroneously inflated the percentage of neuroprotective ferritin expression at this time point; regardless, the lack of Pb-associated increased ferritin at PND 240 in Tg females is suggestive of sex-specific microglial dysfunction.

AD-associated relevant neuronal phenotypes were also preferentially impacted in a sex-biased manner through GxE interactions. The strikingly consistent localization of ferritin-immunopositive microglia within the hippocampal CA3 region (Fig. 2a) was further investigated for aberrations in region-specific neurosupportive signaling through immunostaining of the neurotrophic receptor TrkB on non-microglial cells ($TrkB^{+}/Iba1^{-}$) (Fig. 3a, b). We observed that male mice regardless of genotype had similar Pb-associated changes in CA3 TrkB expression over time, namely, increased TrkB expression at PND 120 compared to controls that was then significantly reduced by PND 240 (Fig. 3c, d), suggesting a greater impact of environmental rather than genetic factors. However, consistent with the microglial phenotype results, potentiative GxE interactions on TrkB expression were readily observable in female mice. Postnatal Pb exposure decreased CA3 TrkB expression WT females at both PND 120 and 240 (Fig. 3c), but significantly increased TrkB in Tg females at PND 120 that decreased over time to similar levels as vehicle-treated mice by PND 240 (Fig. 3d).

Of note, region-specific microglia:neuron signaling through the TrkB receptor is crucial for synaptic plasticity, neuronal survival, and differentiation [31], and is particularly important to long term potentiation (LTP) along the mossy fiber pathway (MFP) [32]. Granule cells from the dentate gyrus project to pyramidal CA3 neurons in the MFP using non-associative LTP, an NMDA-independent form of synaptic plasticity that relies on repeated stimulation and calcium influx to increase the probability of presynaptic glutamate release. Recent studies have demonstrated TrkB signaling is important not only to the development and maintenance of granule cell synaptic connectivity

[33], but also maturation of mossy fiber terminals in terms of number of synaptic vesicles, synaptic contacts, and density of axon distribution [34]. Importantly, TrkB-associated remodeling of the MFP granule cell-CA3 synapse has been shown to promote increased glutamate release, hyperexcitability, and feedforward inhibition to CA3 pyramidal neurons [35], while another study demonstrated an association between stress-induced CA3 glutamate increase and hippocampal atrophy following chronic reductions in adult neurogenesis [36], a hallmark pathology of AD. In addition, both ferritin and amyloid beta have been reported to inhibit glutamate uptake [37,38], increasing the likelihood of excitotoxicity in susceptible neuronal populations. At PND 120, both male and female Pb-exposed Tg mice exhibited phenotypes favorable for a hyperexcitable hippocampal environment, such as increased ferritin (Fig. 2e) and TrkB (Fig. 3d) expression in the CA3 region at an age beyond our previous reports at PND 90 of significantly increased amyloid accumulation [8]. By PND 240, Pb-exposed Tg males retained high ferritin but exhibited a compensatory decrease in TrkB hippocampal expression compared to controls, whereas the excitotoxic-favorable phenotype is relatively maintained at this age in Tg females in spite of continual amyloid accumulation, suggesting that compensatory signals to mediate potential hyperexcitability erode or lose efficacy over time in Pb-exposed Tg females. The present study did not measure any direct evidence of excitotoxicity or hippocampal-specific hyperexcitability, but the significant incongruity in homeostatic neuronal:microglial in GxE females at PND 240 supports our hypothesis and warrants further investigation.

Since synaptic TrkB expression is relatively transient due to protein phosphatases sustained changes to neuronal function, like LTP, consequent to GxE interactions were further explored via analysis of whole brain synaptic protein content. Strikingly, GxE interactions resulted in significant sex bias to synaptic protein expression at PND 120. Pb-exposed Tg females exhibited significant reductions in both SNAP25 (Fig. 4a) and synaptophysin (Fig. 4c), which was not observed in males until PND 240 (Fig. 4b, d), suggesting GxE-associated synaptic aberrations were promoted earlier in females compared to males. Extensive synaptophysin loss is a hallmark of early/mild AD preceding cognitive decline [12], adding support to a GxE-centered hypothesis of female susceptibility to synaptic defects associated with early AD. In the United States, women account for two-thirds of all AD cases [39], highlighting the importance of delineating underlying sex bias in potential mechanisms of disease progression. Relatedly, loss of SNAP25 in the CNS has been reported to produce extensive cell death and neurodegeneration [40,41] and has recently been proposed as a novel biomarker of AD [42].

Notably, the reduction in synaptic proteins in GxE females at PND 120 was not observed at PND 240 (Fig. 4a, c). The significant increase in SNAP25 at this age is likely evidence of neuronal compensation for the previous onslaught of pro-neurodegenerative conditions at PND 120, and further corroborates the hippocampal TrkB expression results at PND 240. Levels of presynaptic proteins, like SNAP25, are regulated by signaling through TrkB, thereby changing the synaptic terminal phenotype [34], so the age-related and sex-specific correlation between the two markers indicates significant changes to synaptic protein content, phenotype, and functionality late in life. In addition, SNAP25 is expressed only at glutamatergic synapses in the CNS, and is critical to regulation of calcium responsiveness and network excitability [43], which would suggest that these GxE female-biased changes in synaptic phenotype promote a hyperexcitable-favorable neuronal environment. However, the M2-dominant microglial phenotype and lack of increased ferritin expression at PND 240 indicate that microglia are not responding appropriately to the same environmental cues, ultimately supporting our hypothesis that female-biased GxE interactions disrupt efficacious microglia:neuron signaling.

Taken together, our data indicate that the combination of genetic and environmental susceptibilities within our AD model act synergistically to promote female bias in the dysregulation of vital interactions between neurons and microglia. Furthermore, the apparent compensatory changes in neuronal parameters, coupled with the increased risk of excitotoxic and microglia-specific vulnerabilities to oxidative damage later in life, indicate that microglia are likely responsible for the majority of maladaptive signaling. Additional investigation is warranted to delineate the mechanisms by which microglia become maladaptive or dysfunctional over time following an early-life exposure during a critical period of sex-specific microglial development. In a similar manner as with cancer, it is compelling to consider hallmark pathologies associated with AD as indicative of failed compensatory responses and maladaptation of key homeostatic cellular populations, such as microglia, rather than evidence of aging-related senescence or metabolic exhaustion. By redirecting the focus of GxE disease paradigms to integrate early microglial dysregulation into later life neuronal crosstalk and signaling maladaptation, it then becomes possible for an entirely new approach to investigating highly complicated, long-term disease etiopathologies like AD.

Conflict of interest

None.

Acknowledgements

The authors would like to acknowledge Dr. Qun Lu of the Harriet and John Wooten Laboratory for Alzheimer's and Neurodegenerative Diseases Research, our funding source, for transgenic mouse accessibility, as well as the East Carolina University Department of Comparative Medicine for their excellent husbandry and care of our animals. We would also like to acknowledge the work of Zoe Hinton and Briana Davidson, ECU Honors Neuroscience students who assisted with portions of synaptosomal purification.

Funding

This work was graciously supported by the Harriet and John Wooten Laboratory for Alzheimer's and Neurodegenerative Diseases Research at East Carolina University.

References

[1] V. Mathew, S.V. Ayyar, Developmental origins of adult diseases, Indian J. Endocrinol. Metab. 16 (4) (2012) 532–541, https://doi.org/10.4103/2230-8210.98005.
[2] M.M. Mielke, P. Vemuri, W.A. Rocca, Clinical epidemiology of Alzheimer's disease: assessing sex and gender differences, Clin. Epidemiol. 6 (2014) 37–48, https://doi.org/10.2147/CLEP.S37929.
[3] D. Holland, R.S. Desikan, A.M. Dale, L.K. McEvoy, Alzheimer's Disease Neuroimaging Initiative, Higher rates of decline for women and apolipoprotein E epsilon4 carriers, AJNR Am. J. Neuroradiol. 34 (12) (2013) 2287–2293.
[4] K.A. Lin, K.R. Choudhury, B.G. Rathakrishnan, et al., Marked gender differences in progression of mild cognitive impairment over 8 years, Alzheimers Dement. 1 (2) (2015) 103–110.
[5] L. Shi, Z. Zhang, B. Su, Sex biased gene expression profiling of human brains at major developmental stages, Sci. Rep. 6 (2016) 21181, , https://doi.org/10.1038/srep21181.
[6] S.D. Bilbo, Early-life infection is a vulnerability factor for aging-related glial alterations and cognitive decline, Neurobiol. Learn. Mem. 94 (2010) 57–64.
[7] J.M. Schwarz, S.D. Bilbo, Sex, glia, and development: interactions in health and disease, Horm. Behav. 62 (3) (2012) 243–253, https://doi.org/10.1016/j.yhbeh.2012.02.018.
[8] A.N. vonderEmbse, Q. Hu, J.C. DeWitt, Developmental toxicant exposure in a mouse model of Alzheimer's disease induces differential sex-associated microglial activation and increased susceptibility to amyloid accumulation, J. Dev. Orig. Health Dis. (2017) 1–9, https://doi.org/10.1017/S2040174417000277.
[9] A. Bessis, C. Béchade, D. Bernard, A. Roumier, Microglial control of neuronal death and synaptic properties, Glia 55 (3) (2007) 233–238, https://doi.org/10.1002/glia.20459.
[10] P.A. Garay, A.K. McAllister, Novel roles for immune molecules in neural development: implications for neurodevelopmental disorders, Front. Synaptic Neurosci. 2 (2010) 136, https://doi.org/10.3389/fnsyn.2010.00136.
[11] H. Du, L. Guo, S. Yan, A.A. Sosunov, G.M. McKhann, S.S.D. Yan, Early deficits in synaptic mitochondria in an Alzheimer's disease mouse model, Proc. Natl. Acad. Sci.

U. S. A. 107 (43) (2010) 18670–18675.
[12] E. Masliah, M. Mallory, M. Alford, R. DeTeresa, L.A. Hansen, D.W. McKeel Jr., J.C. Morris, Altered expression of synaptic proteins occurs early during progression of Alzheimer's disease, Neurology 56 (1) (2001) 127–129.
[13] M.E.R. Butchbach, J.D. Edwards, K.R. Schussler, A.H.M. Burghes, A novel method for oral delivery of drug compounds to the neonatal SMNΔ7 mouse model of spinal muscular atrophy, J. Neurosci. Methods 161 (2) (2007) 285–290, https://doi.org/10.1016/j.jneumeth.2006.11.002.
[14] J. Schindelin, I. Arganda-Carreras, E. Frise, Fiji: an open-source platform for biological-image analysis, Nat. Methods 9 (7) (2012) 676–682.
[15] Y. Tang, W. Le, Differential roles of M1 and M2 microglia in neurodegenerative diseases, Mol. Neurobiol. 53 (2015) 1181, https://doi.org/10.1007/s12035-014-9070-5.
[16] J. Yamada, H. Nakanishi, S. Jinno, Differential involvement of perineuronal astrocytes and microglia in synaptic stripping after hypoglossal axotomy, Neuroscience 182 (2011) 1–10, https://doi.org/10.1016/j.neuroscience.2011.03.030.
[17] C. Quintana, L. Gutiérrez, Could a dysfunction of ferritin be a determinant factor in the aetiology of some neurodegenerative diseases? Biochim. Biophys. Acta 1800 (2010) 770–782.
[18] T. Bolmont, F. Haiss, D. Eicke, R. Radde, C.A. Mathis, W.E. Klunk, S. Kohsaka, M. Jucker, M.E. Calhoun, Dynamics of the microglial/amyloid interaction indicate a role in plaque maintenance, J. Neurosci. 28 (16) (2008) 4283–4292.
[19] X.G. Luo, S.D. Chen, The changing phenotype of microglia from homeostasis to disease, Transl. Neurodegener. 1 (2012) 9.
[20] J.M. Crain, M. Nikodemova, J.J. Watters, Microglia express distinct M1 and M2 phenotypic markers in the postnatal and adult central nervous system in male and female mice, J. Neurosci. Res. 91 (2013) 1143–1151.
[21] D.C. Lee, C.R. Ruiz, L. Lebson, M.J.B. Selenica, J. Rizer, J.B. Hunt Jr., R. Rojiani, P. Reid, S. Kammath, K. Nash, C.A. Dickey, M. Gordon, D. Morgan, Aging enhances classical activation but mitigates alternative activation in the central nervous system, Neurobiol. Aging 34 (6) (2013) 1610–1620.
[22] Y. Nakagawa, K. Chiba, Role of microglial M1/M2 polarization in relapse and remission of psychiatric disorders and diseases, Pharmaceuticals (Basel) 7 (2014) 1028–1048, https://doi.org/10.3390/ph7121028.
[23] S. Prokop, K.R. Miller, F.L. Heppner, Microglia actions in Alzheimer's disease, Acta Neuropathol. 126 (2013) 461–477.
[24] V.H. Perry, J. Teeling, Microglia and macrophages of the central nervous system: the contribution of microglia priming and systemic inflammation to chronic neurodegeneration, Semin. Immunopathol. 35 (2013) 601–612, https://doi.org/10.1007/s00281-013-0382-8.
[25] V.H. Perry, J.A.R. Nicoll, C. Holmes, Microglia in neurodegenerative disease, Nat. Rev. Neurol. 6 (2010) 193–201.
[26] J. Vinet, H.R.J. van Weering, A. Heinrich, R.E. Kälin, A. Wegner, N. Brouwer, F.L. Heppner, N. van Rooijen, H. WGM Boddeke, K. Biber, Neuroprotective function for ramified microglia in hippocampal excitotoxicity, J. Neuroinflammation 9 (2012) 27, https://doi.org/10.1186/1742-2094-9-27.
[27] D.A. Simmons, M. Casale, B. Alcon, N. Pham, N. Narayan, G. Lynch, Ferritin accumulation in dystrophic microglia is an early event in the development of Huntington's disease, Glia 55 (2007) 1074–1084.
[28] K.O. Lopes, D.L. Sparks, W.J. Streit, Microglia dystrophy in the aged and Alzheimer's disease brain is associated with ferritin immunoreactivity, Glia 56 (2008) 1048–1060.
[29] J.T. Rogers, A.I. Bush, H.H. Cho, D.H. Smith, A.M. Thomas, A.L. Friedlich, D.K. Lahiri, P.J. Leedman, X. Huang, C.M. Cahill, Iron and the translation of the amyloid precursor protein (APP) and ferritin mRNAs: riboregulation against neural oxidative damage in Alzheimer's disease, Biochem. Soc. Trans. 36 (2008) 1282–1287, https://doi.org/10.1042/BST0361282.
[30] A. Kroner, A.D. Greenhalgh, J.G. Zarruk, R. Passos dos Santos, M. Gaestel, S. David, TNF and increased intracellular iron alter macrophage polarization to a detrimental M1 phenotype in the injured spinal cord, Neuron 83 (5) (2014) 1098–1116.
[31] A. Yoshii, M. Constantine-Paton, Postsynaptic BDNF-TrkB signaling in synapse maturation, plasticity, and disease, Dev. Neurobiol. 70 (5) (2010) 304–322.
[32] S. Schidlt, T. Endres, V. Lessmann, E. Edelmann, Acute and chronic interference with BDNF/TrkB-signaling impair LTP selectively at mossy fiber synapses in the CA3 region of the mouse hippocampus, Neuropharmacology 71 (2013) 247–254.
[33] S.C. Danzer, R.J. Kotloski, C. Walter, M. Hughes, J.O. McNamara, Altered morphology of hippocampal dentate granule cell presynaptic and postsynaptic terminals following conditional deletion of TrkB, Hippocampus 18 (2008) 668–678.
[34] R. Otal, A. Martínez, E. Soriano, Lack of TrkB and TrkC signaling alters the synaptogenesis and maturation of mossy fiber terminals in the hippocampus, Cell Tissue Res. 319 (2005) 349–358.
[35] P.B. Bernard, D.S. MacDonald, D.A. Gill, C.L. Ryan, R.A. Tasker, Hippocampal mossy fiber sprouting and elevated trkB receptor expression following systemic administration of low dose domoic acid during neonatal development, Hippocampus 17 (11) (2007) 1121–1133.
[36] R.J. Schloesser, D.V. Jimenez, N.F. Hardy, D. Paredes, B.J. Catlow, H.K. Manji, R.D. McKay, K. Martinowich, Atrophy of pyramidal neurons and increased stress-induced glutamate levels in CA3 following chronic suppression of adult neurogenesis, Brain Struct. Funct. 219 (2014) 1139–1148.
[37] A.V. Alekseenko, T.V. Waseem, S.V. Fedorovich, Ferritin, a protein containing iron nanoparticles, induces reactive oxygen species formation and inhibits glutamate uptake in rat brain synaptosomes, Brain Res. 1241 (2008) 193–200.
[38] S. Li, S. Hong, N.E. Shepardson, et al., Soluble oligomers of amyloid β protein facilitate hippocampal long-term depression by disrupting neuronal glutamate uptake, Neuron 62 (6) (2009) 788–801, https://doi.org/10.1016/j.neuron.2009.05.012.
[39] L.E. Hebert, J. Weuve, P.A. Scherr, D.A. Evans, Alzheimer disease in the United States (2010-2050) estimated using the 2010 census, Neurology 80 (19) (2013) 1778–1783.
[40] T.C. Santos, K. Wierda, J.H. Broeke, R.F. Toonen, M. Verhage, Early golgi abnormalities and neurodegeneration upon loss of presynaptic proteins Munc18-1, syntaxin-1 or SNAP-25, J. Neurosci. 27 (2017) 3352–3356, https://doi.org/10.1523/jneurosci.3352-16.2017.
[41] M. Sharma, J. Burré, P. Bronk, Y. Zhang, W. Xu, T.C. Südhof, CSPα knockout causes neurodegeneration by impairing SNAP-25 function, EMBO J. 31 (2012) 829–841.
[42] A. Brinkmalm, G. Brinkmalm, W.G. Honer, et al., SNAP-25 is a promising novel cerebrospinal fluid biomarker for synapse degeneration in Alzheimer's disease, Mol. Neurodegener. (2014) 53, https://doi.org/10.1186/1750-1326-9-53.
[43] C. Verderio, D. Pozzi, E. Pravettoni, et al., SNAP-25 modulation of calcium dynamics underlies differences in GABAergic and glutamatergic responsiveness to depolarization, Neuron 41 (4) (2004) 599–610, https://doi.org/10.1016/S0896-6273(04)00077-7.